The 2011 La Niña: So Strong, the Oceans Fell

Carmen Boening[1], Josh K. Willis[1], Felix W. Landerer[1], R. Steven Nerem[2], John Fasullo[3]

[1] *Jet Propulsion Laboratory, California Institute of Technology, 4800 Oak Grove Dr., Pasadena, California 91109, USA.*

[2] *Colorado Center for Astrodynamics Research, University of Colorado, Boulder, Colorado, USA*

[3] *National Center for Atmospheric Research, Boulder, Colorado, USA*

carmen.boening@jpl.nasa.gov

Global mean sea level (GMSL) dropped by 5 mm between the beginning of 2010 and mid 2011. This drop occurred despite the background rate of rise, 3 mm per year, which dominates most of the 18-year record observed by satellite altimeters. Using a combination of satellite and in situ data, we show that the decline in ocean mass, which explains 60 % of the sea level drop, coincides with an equivalent increase in terrestrial water storage, primarily over Australia, the Amazon basin, and Southeast Asia. This temporary shift of water from the ocean to land is closely related to the transition from El Niño conditions in 2009/10 to a strong 2010/11 La Niña, which affected precipitation patterns world-wide. The excess transport of water from the ocean represents a 3 % increase over the long-term climatological value. This study presents the first direct observation of the ENSO-induced exchange of freshwater that drives interannual changes in GMSL. Understanding these short-term changes helps to separate natural variability from anthropogenic and will ultimately provide a foundation for improved sea level predictions.

Observations from satellite altimeters, along with tide gauge data since the late 19th Century, reveal a fairly steady increase in global mean sea level (GMSL) of about 1.7 mm/year, with a modest acceleration detectable over the 130 year record [1]. The rising seas have already had impacts on coastal infrastructure and the potential for future socioeconomic impacts is very high, yet very uncertain [2]. Understanding the causes of modern day GMSL change and distinguishing natural and anthropogenic variations is therefore a top scientific priority.

Since the early 1990s, satellite altimeter observations have made it possible to distinguish interannual variations of several millimeters in amplitude from the background rate of GMSL rise [3]. Although a great deal of uncertainty remains regarding future projections of global sea level rise, almost all projections imply a significant acceleration during the 21st Century [4-7]. In order to distinguish such longer-term accelerations from natural variations in GMSL, it is necessary to understand the causes of these interannual variations. As natural variations in GMSL can be explained and quantified, satellite altimeter observations will become a key indicator of anthropogenic influence on the global climate.

Recent studies have indicated that interannual fluctuations in GMSL are connected to the tropical El Niño Southern Oscillation (ENSO) [3, 8], which influences ocean surface temperatures in the tropical Pacific as well as evaporation and precipitation patterns globally. In 2010, the Central Pacific El Nino evolved into a strong La Niña, leading to a decrease in upper ocean temperatures in the eastern Pacific and higher temperatures in the western tropical Pacific [9]. During this time, the altimetry record shows a significant drop of approximately 5 mm in GMSL within a period of about 16 months (Fig. 1).

Interannual changes in GMSL can be attributed to changes in the ocean's mass or its heat content. The Gravity Recovery and Climate Experiment (GRACE) satellites are capable of measuring changes in the mass of the ocean on monthly time scales with an accuracy of a few millimeters. The Argo array of profiling floats observes changes in the volume averaged temperature of the upper ocean with an accuracy that allows the thermosteric contribution to GMSL change to be computed with similar accuracy [10]. To complement the ARGO estimates, we also provide an independent estimate of changes in ocean heat content from top of the atmosphere radiation estimates from CERES. Using these four independent observing systems, we can attribute the changes in GMSL to their root causes [11]. The combination of the new observing systems – available after 2005 - allows for direct observations of all of the contributions to ENSO-related sea level change, and the relative importance of heat exchange and water mass transport. Previous studies either inferred the relative contributions [12] or modeled one of the components [8].

Figure 1 indicates that the drop starts in mid-2010, concurrent with the onset of La Nina (Figure 3S). The 5 mm decrease in GMSL from March 2010 to May 2011 is largely explained by a decrease in global ocean mass of 3 mm (about 1100 Gt of mass) during this period (Fig. 2). Thermosteric sea level is almost unchanged over this period. Argo observations show cooling of about 2 mm near the beginning of 2010 and a small increase of approximately 1 mm in May of 2011, near the end of the La Niña event. The decrease in ocean mass lags the cooling, beginning in mid 2010 near the peak of the La Niña event. It is clear from the close agreement between ocean mass and sea level observations during this period that loss of mass from the ocean was the primary cause of the 2010 drop in GMSL. The CERES estimate of net radiation (Fig. 1,

dashed line) confirms that any cooling of the ocean across the 2010 drop is likely to be small and unable to account for most of the the altimetry signal.

Given that the atmospheric contribution to the total mass in the form of water vapor is small on interannual time scales (<1mm [13]), the significant loss in ocean mass coincides with a mass gain of a comparable amount over land. We use GRACE satellite gravity observations to diagnose changes in terrestrial water storage (TWS) [14-16]. Figure 3 shows that TWS over the northern part of South America and Australia substantially increased by early 2011 compared to 2010. Southeast Asia also gained water over this period. It is worth noting that both South America and South-East Asia suffered larger water deficits in the prior year (Figure 1S), due to the El Niño event in 2009/10 and thus are significant contributors to the oceanic mass loss as precipitation replenished these regions, which had experienced intense drought.

Data from the Tropical Rainfall Measuring Mission (TRMM) indicates that most of the observed mass gain is consistent with a significant change in rainfall during the period from 2010 to 2011 (Fig. 2S). Precipitation patterns over regions such as South America, Australia, and Southeast Asia are highly affected by ENSO [17]. During La Niña episodes, rainfall is enhanced across the western equatorial Pacific, Indonesia and the Philippines and is nearly absent across the eastern equatorial Pacific. Wetter than normal conditions tend to be observed from December through February over northern South America and southern Africa, and from June through August over southeastern Australia. During El Niño, dryer than normal conditions typically exist in South America and southeast Asia. TRMM data reflect the transition El Niño to La Niña during 2010, with the regions of enhanced precipitation corresponding well with the regions of increased TWS (Figure 2S). This indicates a strong connection between the transition to the 2010/11 La Nina, the changes in TWS and mass related sea level.

To quantify this, Figure 4 shows fluctuations in TWS in the regions that are most strongly affected, expressed in terms of their impact on global ocean mass. Averages over Australia and Indonesia, South America, and Southeast Asia indicate that most of the TWS gain was accumulated in these regions. Other regions account mostly for short-term variability, apart from Greenland and Antarctica, which consistently lose mass over the entire GRACE record. The sum of TWS storage in Australia and Indonesia, South America and Southeast Asia is equivalent to a total mass increase of about 3 mm of GMSL equivalent height between March 2010 and May 2011 (Fig. 4 b). This 3 mm drop in ocean mass represents a small but significant fraction of the net water transport from ocean to land, a key part of the global hydrologic cycle. On average, the atmosphere delivers 40 x 10^3 km^3 of water to the land [18], which is returned as runoff. This is equivalent to 12 cm of global sea level change per year. Thus, the 3 mm drop represents a change of approximately 3 % in climatological rate of water transport from the oceans onto the land.

The time series of ENSO events represented by the Multivariate ENSO Index (MEI) indicates that the 2010/11 La Niña was the strongest over the altimetry period starting in 1992 – and one of the strongest La Niña events for that season in the last 60 years. Flooding events in Australia, Pakistan and China have been associated with the 2010/11 La Niña and also with record high SSTs in the Arabian Sea and north of Australia [19]. The cumulative influence of related synoptic events appears to have transported enough water to the continents to explain 60 % of the 2010 drop in GMSL. The connection to ENSO suggests a rather short-lived hiatus in GMSL rise. Indeed, the most recent data suggest a recovery of about 2 mm in the last few months of the GMSL time series. ENSO-driven changes in GMSL like the one described here might mask GMSL variations related to anthropogenic forcing over short time periods, but as

expected from the lag of continental freshwater outflows relative to precipitation anomalies, they are unable to curtail the longer timescale trends associated with persistent ice melt and ocean warming as observed in recent decades. In summary, we have presented the first direct observations of a 5 mm drop in GMSL driven by an ENSO-related transfer of mass between the oceans and the continents. Observational closure of the sea level budget provides strong evidence that interannual changes in GMSL on the order of half a centimeter can be driven by this mechansim. During 2010, the 5 mm drop in GMSL was driven by the transition from an El Niño to strong La Niña that peaked in late 2010 and early 2011. In contrast, the thermosteric component of this event was very small. Predicting future rates of sea level change and detecting any acceleration in GMSL rise will require the ability to distinguish such events from increases in the net heat content of the ocean, as well as rapid changes in the amount of ice lost from the glaciers and ice sheets. This underscores the importance of complementary global observing systems such as Jason, GRACE and Argo, without which such distinctions would be impossible.

Methods summary

Global mean sea level is computed using a weighted average of along track data from TOPEX/Poseidon, Jason-1 and Jason-2. All standard corrections according to [3] have been applied and time series has been smoothed with a 60-day boxcar filter to remove a spurious 59-day cycle in the data [20].

Global mean ocean mass is computed from GRACE, using Release-04 data from CSR. We omit data that is within 300km of coastal areas [21], and apply corrections for geocenter motion [22] as well as for C(2,0) [23] as recommended by the GRACE project. Trends associated with

glacial isostatic adjustment are subtracted from the GRACE solutions [24]. The maps of TWS were filtered for correlated errors [25], and smoothed with a 500 km Gaussian filter.

Maps of thermosteric sea level are calculated as detailed in [10]. Monthly maps are estimated relative to a regionally varying climatology and seasonal cycle, using thermosteric sea level anomalies between the surface and 900 m computed from individual Argo profiles. The covariance function and noise-to-signal ratio are the same as those used by [10].

The net flux at the top-of-atmosphere is computed from CERES-EBAF v2.6 fluxes through 2010 and extended with the CERES Flashflux dataset through September 2011 [26] . The timeseries are combined based on adjusting the mean flux from Flashflux data to agree with that from EBAF from Jan. 2009 through Dec. 2010.

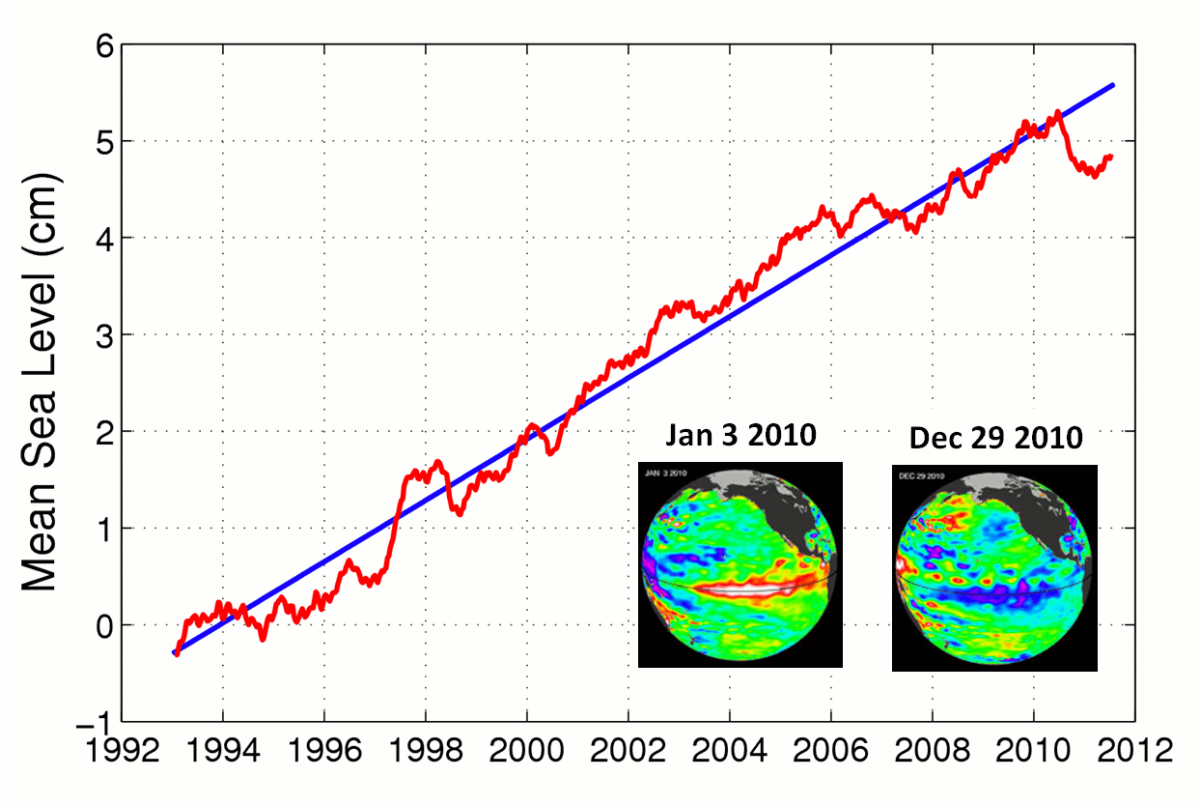

Figure 1: Global mean sea level from altimetry from 1992 to 2011 with annual and semi-annual variations removed and smoothed with a 60-day running mean filter [3]. The slope of the trend (blue line) is 3.2 mm/year after a GIA correction has been applied (0.3 mm/year). The insets show maps of SSH anomaly relative to the background trend and seasonal climatology, for 10-day averages centered on Jan 3 2010 (near the peak of the El Niño) and Dec 29 2010 (the peak of La Niña).

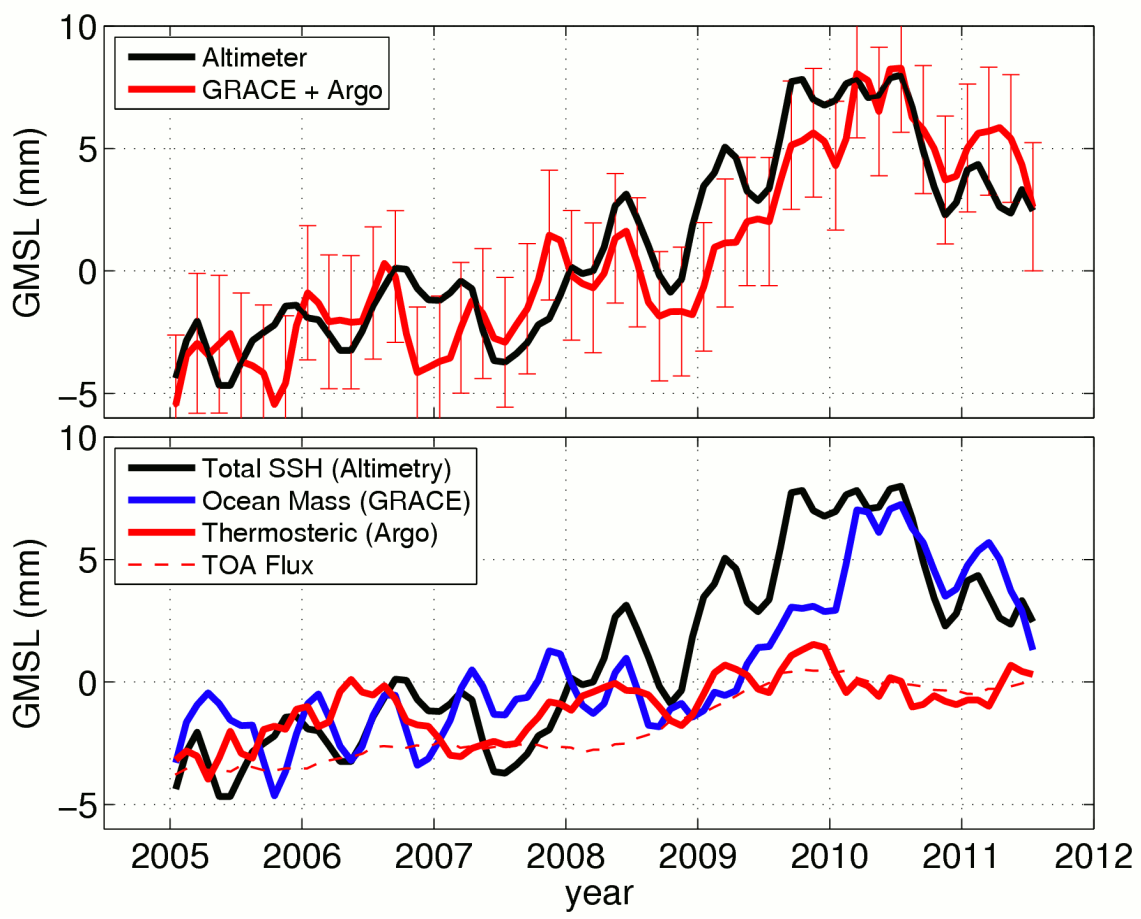

Figure 2: (top panel) Global mean sea level from altimetry from 2005 to mid-2011 (black line). The red line shows the sum of the ocean mass contribution (as measured by GRACE) and thermal expansion contribution (as measured by Argo). Error bars are 2.5 mm (as discussed in the Methods Section). (bottom panel) Contributions to global sea level rise from 2005 to mid-2011. As in the top panel, the black line shows GMSL as observed by satellite altimeters. Ocean mass changes are shown in blue and thermosteric sea level change is shown in red. . The red dashed line shows an estimate of ocean warming based on estimates of radiative imbalance at the top of the atmosphere. The mean warming rate is adjusted to agree with Argo and heat content is scaled assuming that 3×10^{22} J is equivalent to 5 mm of thermosteric sea level rise as in [27].

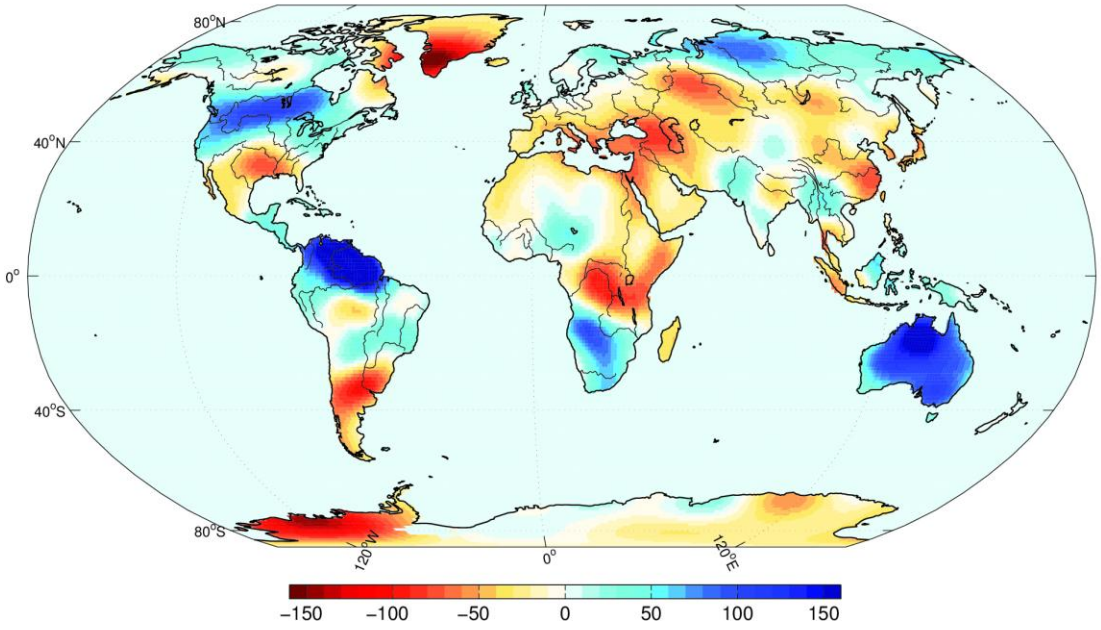

Figure 3: Change in water mass from beginning of 2010 (JFM average) to mid 2011 (MAM average). Blue colors indicate an increase in water mass over the continents.

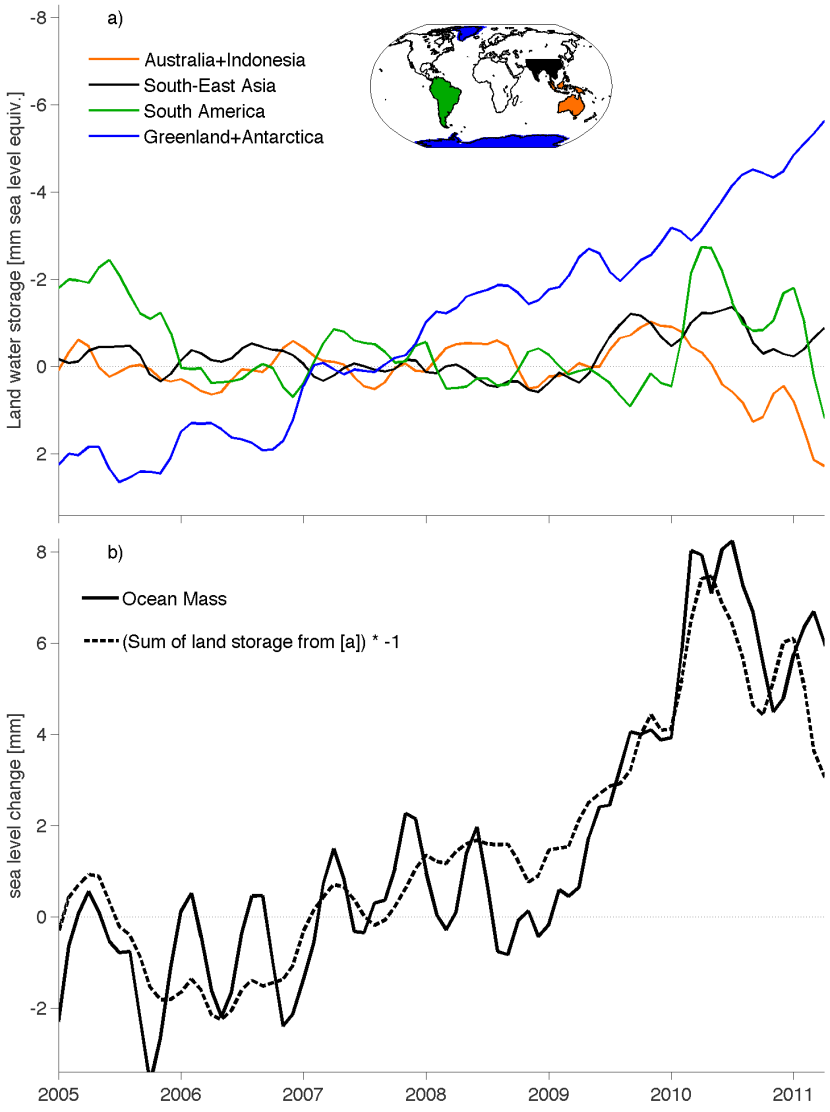

Figure 4: (a) TWS (terrestrial water storage) for the regions that played a significant role in the 2010 drop in GMSL. Mass loss in Greenland and Antarctica are also shown. The amount of TWS expressed in units of equivalent sea level change. Note that the vertical axis is reversed for ease of comparison with ocean mass increase (b) The sum of TWS over the regions plotted in (a) along with the integral over all other land regions. For comparison, global ocean mass increase is also shown.

References

1. Church, J.A. and N.J. White, *Sea-Level Rise from the Late 19th to the Early 21st Century*. Surveys in Geophysics, 2011. **32**(4-5): p. 585-602.
2. Nicholls, R.J., et al., *Sea-level rise and its possible impacts given a 'beyond 4 degrees C world' in the twenty-first century*. Philosophical Transactions of the Royal Society a-Mathematical Physical and Engineering Sciences, 2011. **369**(1934): p. 161-181.
3. Nerem, R.S., et al., *Estimating Mean Sea Level Change from the TOPEX and Jason Altimeter Missions*. Marine Geodesy, 2010. **33**: p. 435-446.
4. Rahmstorf, S., *A semi-empirical approach to projecting future sea-level rise*. Science, 2007. **315**(5810): p. 368-370.
5. Vermeer, M. and S. Rahmstorf, *Global sea level linked to global temperature*. Proceedings of the National Academy of Sciences of the United States of America, 2009. **106**(51): p. 21527-21532.
6. Grinsted, A., J.C. Moore, and S. Jevrejeva, *Reconstructing sea level from paleo and projected temperatures 200 to 2100 ad*. Climate Dynamics, 2010. **34**(4): p. 461-472.
7. Meehl, G.A., et al., *Global Climate Projections*., in *Climate Change 2007: The Physical Science Basis*. *Contribution of Working Group I to the Fourth Assessment Report of the Intergovernmental Panel on Climate Change*, S. Solomon, D. Qin, M. Manning, Z. Chen, M. Marquis, K.B. Averyt, M. Tignor and H.L. Miller, Editor 2007, Cambridge University Press: Cambridge, United Kingdom and New York, NY, USA.
8. Ngo-Duc, T., et al., *Contribution of continental water to sea level variations during the 1997-1998 El Nino-Southern Oscillation event: Comparison between Atmospheric Model Intercomparison Project simulations and TOPEX/Poseidon satellite data*. Journal of Geophysical Research-Atmospheres, 2005. **110**(D9).
9. Bell, G.D., M. Halpert, and M. L'Heureux, *[The Tropics] ENSO and the Tropical Pacific [in State of the Climate in 2010]*. Bulletin of the American Meteorological Society, 2011. **92**(6): p. S109-S114.
10. Willis, J.K., D.P. Chambers, and R.S. Nerem, *Assessing the globally averaged sea level budget on seasonal to interannual timescales*. Journal of Geophysical Research-Oceans, 2008. **113**(C6).
11. Leuliette, E.W. and J.K. Willis, *Balancing the Sea Level Budget*. Oceanography, 2011. **24**(2): p. 122-129.
12. Willis, J.K., D. Roemmich, and B. Cornuelle, *Interannual variability in upper ocean heat content, temperature, and thermosteric expansion on global scales*. Journal of Geophysical Research-Oceans, 2004. **109**(C12).
13. Landerer, F.W., J.H. Jungclaus, and J. Marotzke, *El Nino-Southern Oscillation signals in sea level, surface mass redistribution, and degree-two geoid coefficients*. Journal of Geophysical Research-Oceans, 2008. **113**(C8).
14. Swenson, S., et al., *A comparison of terrestrial water storage variations from GRACE with in situ measurements from Illinois*. Geophysical Research Letters, 2006. **33**(16).
15. Rodell, M., et al., *Estimating groundwater storage changes in the Mississippi River basin (USA) using GRACE*. Hydrogeology Journal, 2007. **15**(1): p. 159-166.
16. Syed, T.H., et al., *Analysis of terrestrial water storage changes from GRACE and GLDAS*. Water Resources Research, 2008. **44**(2).
17. Hoerling, M.P. and A. Kumar, *Understanding and predicting extratropical teleconnections related to ENSO*. *In El Niño and the Southern Oscillation: Multi-scale Variations and Global and Regional Impacts*, H.F. Diaz and V. Markgraf, Editors. 2000, Cambridge University Press. p. 57-88.
18. Trenberth, K.E., et al., *Estimates of the global water budget and its annual cycle using observational and model data*. Journal of Hydrometeorology, 2007. **8**(4): p. 758-769.

19. Trenberth, K.E. and J. Fasullo, *Climate extremes and climate change: The Russian Heat Wave and other Climate Extremes*. Journal of Climate, 2011. **in review**.
20. Leuliette, E.W., R.S. Nerem, and G.T. Mitchum, *Calibration of TOPEX/Poseidon and Jason Altimeter Data to Construct a Continuous Record of Mean Sea Level Change*. Marine Geodesy, 2004. **27**(1-2): p. 79-94.
21. Chambers, D.P., *Evaluation of new GRACE time-variable gravity data over the ocean*. Geophysical Research Letters, 2006. **33**(17).
22. Swenson, S., D. Chambers, and J. Wahr, *Estimating geocenter variations from a combination of GRACE and ocean model output*. Journal of Geophysical Research-Solid Earth, 2008. **113**(B8).
23. Cheng, M.K. and B.D. Tapley, *Variations in the Earth's oblateness during the past 28 years*. Journal of Geophysical Research-Solid Earth, 2004. **109**(B9).
24. Paulson, A., S.J. Zhong, and J. Wahr, *Inference of mantle viscosity from GRACE and relative sea level data*. Geophysical Journal International, 2007. **171**(2): p. 497-508.
25. Swenson, S. and J. Wahr, *Post-processing removal of correlated errors in GRACE data*. Geophysical Research Letters, 2006. **33**(8).
26. Loeb, N.G., et al., *Toward Optimal Closure of the Earth's Top-of-Atmosphere Radiation Budget*. Journal of Climate, 2009. **22**(3): p. 748-766.
27. Church, J.A., N.J. White, and J.M. Arblaster, *Significant decadal-scale impact of volcanic eruptions on sea level and ocean heat content*. Nature, 2005. **438**(7064): p. 74-77.
28. Leuliette, E.W. and L. Miller, *Closing the sea level rise budget with altimetry, Argo, and GRACE*. Geophysical Research Letters, 2009. **36**.

Supplementary Information is linked to the online version of the paper at www.nature.com/nature.

Acknowledgements

The work was performed at the Jet Propulsion Laboratory, California Institute of Technology, under contract with NASA and is partially sponsored by NASA Award NNX09AH89G-S01 and NNG06GB91G. We thank the GRACE analysis centers at University of Texas, JPL, and Geoforschungszentrum Potsdam, and the German Space Operations Center (GSOC) of the German Aerospace Center (DLR).

Author contributions

C.B. designed the study and conducted the research. J.W. computed the steric contribution from ARGO data and provided uncertainty estimates for GRACE+ARGO. F.L. and C.B. calculated terrestrial water storage and ocean mass changes from GRACE data. R.S.N. provided the estimate of global mean sea level from altimetry. J.F. provided estimates of CERES net radiation to relate to ARGO heat content. C.B. and J.W. prepared the manuscript. All authors discussed the results and implications, commented on, and contributed to the manuscript at all stages.

Author Information

Correspondence and requests for materials should be addressed to carmen.boening@jpl.nasa.gov.

Figure Captions

Figure 1: Global mean sea level from altimetry from 1992 to 2011 with annual and semi-annual variations removed and smoothed with a 60-day running mean filter [3]. The slope of the trend (blue line) is 3.2 mm/year after a GIA correction has been applied (0.3 mm/year). The insets show maps of SSH anomaly relative to the background trend and seasonal climatology, for 10-day averages centered on Jan 3 2010 (near the peak of the El Niño) and Dec 29 2010 (the peak of La Niña).

Figure 2: (top panel) Global mean sea level from altimetry from 2005 to mid-2011 (black line). The red line shows the sum of the ocean mass contribution (as measured by GRACE) and thermal expansion contribution (as measured by Argo). Error bars are 2.5 mm (as discussed in the Methods Section). (bottom panel) Contributions to global sea level rise from 2005 to mid-2011. As in the top panel, the black line shows GMSL as observed by satellite altimeters. Ocean mass changes are shown in blue and thermosteric sea level change is shown in red. . The red dashed line shows an estimate of ocean warming based on estimates of radiative imbalance at the top of the atmosphere. The mean warming rate is adjusted to agree with Argo and heat content is scaled assuming that 3×10^{22} J is equivalent to 5 mm of thermosteric sea level rise as in [27].

Figure 3: Change in water mass from beginning of 2010 (JFM average) to mid 2011 (MAM average). Blue colors indicate an increase in water mass over the continents.

Figure 4: (a) TWS (terrestrial water storage) for the regions that played a significant role in the 2010 drop in GMSL. Mass loss in Greenland and Antarctica are also shown. The amount of TWS expressed in units of equivalent sea level change. Note that the vertical axis is reversed for ease of comparison with ocean mass increase (b) The sum of TWS over the regions plotted in (a) along with the integral over all other land regions. For comparison, global ocean mass increase is also shown.

Methods

GRACE data

We estimate the global mean ocean mass using GRACE data derived from the CSR RL04 time variable gravity field solutions. The data have been corrected for geocenter motion using estimates by [22]; glacial isostatic adjustment is subtracted from the GRACE solutions using the model of [24]. The $C_{2,0}$ spherical harmonic coefficients, describing the Earth's oblateness, derived from satellite laser ranging measurements using the estimates by [23] are substituted for the $C_{2,0}$ coefficients in the GRACE product.

The impact of land signals on the GRACE oceanic mass estimates are reduced by applying a land mask omitting data over land and within 300 km from the coast[21]. An inverse mask has been used to derive averages of TWS. The maps of TWS were filtered for correlated errors using the method by [25] and smoothed using a 500 km Gaussian filter.

Altimetric sea level

Maps of sea level anomaly shown inset in Figure 1 are computed using alongtrack data from TOPEX/Poseidon, Jason-1 and Jason-2 observations. A seasonal cycle and trend computed over the period 1993-2008 has been removed and a Gaussian spatial smoothing filter of 2 degrees longitude by 1 degree latitude has been used to produce the maps. Each map represents a 10-day average centered on the date shown.

Global mean sea level is computed using a weighted average of along track data from TOPEX/Poseidon, Jason-1 and Jason-2. The weights are chosen to account for increased data density at height latitudes and all standard corrections have been applied [3]. The time series has been smoothed with a 60-day boxcar filter to remove a spurious 59-day cycle in the data [20].

Steric sea level from ARGO

Maps of thermosteric sea level are calculated as detailed in [10]. Monthly maps are estimated relative to a regionally varying climatology and seasonal cycle, using thermosteric sea level anomalies between the surface and 900 m computed from individual Argo profiles. The covariance function and noise-to-signal ratio are the same as those used by [10].

Uncertainty in the sum of sea level components

Uncertainties shown in Figure 2a reflect the combined uncertainty in Argo estimates of globally averaged thermosteric sea level and GRACE estimates of ocean mass. For the monthly averages, uncertainty in ocean mass is estimated to be approximately 2 mm and uncertainties in thermosteric sea level range from 2.9 to 2.4 mm, consistent with [10] and [28]. The uncertainties in the sum of these components are calculated under the assumption that errors in Argo and GRACE observations are uncorrelated (total error ^{2} = GRACE error^2 + Argo error^2). The errors bars shown in Figure 2a have been reduced by sqrt(2) to account for the 60-day smoothing. The RMS difference between the GMSL curve and the GRACE + Argo curve is 1.5 mm, suggesting that the uncertainties presented here may be overly conservative.

CERES Fluxes

The net flux at the top-of-atmosphere is computed from CERES-EBAF v2.6 fluxes through 2010 and extended with the CERES Flashflux dataset through September 2011 [26] . The timeseries are combined based on adjusting the mean flux from Flashflux data to agree with that from EBAF from Jan. 2009 through Dec. 2010. The CERES mean flux is then adjusted to agree with the mean ARGO tendency from 2005 through 2010.

TRMM precipitation

The TRMM Multi-Satellite Precipitation Analysis (TMPA; computed at monthly intervals as 3B-43) combines the estimates generated by the TRMM and other satellites product (3B-42) and the CAMS global gridded rain gauge data, produced by NOAA's Climate Prediction Center and/or the global rain gauge product produced by the Global Precipitation Climatology Center (GPCC). The output is rainfall for 0.25x0.25 degree grid boxes for each month. The geographic coverage is 50 S to 50 N.